Vibrational Spectrum of the Lumi Intermediate in the Room Temperature Rhodopsin Photo-Reaction

Laszlo Ujj, Frank Jäger, and George H. Atkinson
Department of Chemistry and Optical Science Center, University of Arizona, Tucson, Arizona 85721

ABSTRACT The vibrational spectrum (650–1750 cm^{-1}) of the lumi-rhodopsin (lumi) intermediate formed in the microsecond time regime of the room-temperature rhodopsin (Rh^{RT}) photoreaction is measured for the first time using picosecond time-resolved coherent anti-Stokes Raman spectroscopy (PTR/CARS). The vibrational spectrum of lumi is recorded 2.5 μs after the 3-ps, 500-nm excitation of Rh^{RT}. Complementary to Fourier transform infrared spectra recorded at Rh sample temperatures low enough to freeze lumi, these PTR/CARS results provide the first detailed view of the vibrational degrees of freedom of room-temperature lumi ($lumi^{RT}$) through the identification of 21 bands. The exceptionally low intensity (compared to those observed in $batho^{RT}$) of the hydrogen out-of-plane (HOOP) bands, the moderate intensity and absolute positions of C-C stretching bands, and the presence of high-intensity C═C stretching bands suggest that $lumi^{RT}$ contains an almost planar (nontwisting), all-*trans* retinal geometry. Independently, the 944-cm^{-1} position of the most intense HOOP band implies that a resonance coupling exists between the out-of-plane retinal vibrations and at least one group among the amino acids comprising the retinal binding pocket. The formation of $lumi^{RT}$, monitored via PTR/CARS spectra recorded on the nanosecond time scale, can be associated with the decay of the blue-shifted intermediate (BSI^{RT}) formed in equilibrium with the $batho^{RT}$ intermediate. PTR/CARS spectra measured at a 210-ns delay contain distinct vibrational features attributable to BSI^{RT}, which suggest that the all-*trans* retinal in both BSI^{RT} and $lumi^{RT}$ is strongly coupled to part of the retinal binding pocket. With regard to the energy storage/transduction mechanism in Rh^{RT}, these results support the hypothesis that during the formation of $lumi^{RT}$, the majority of the photon energy absorbed by Rh^{RT} transfers to the apoprotein opsin.

INTRODUCTION

Rhodopsin (Rh), the most widely found photoreceptor within the rod and cone cells in vertebrates, as well as in most invertebrates, is recognized as the fundamental molecular entity by which visual processes function. Rh transmembrane proteins (e.g., bovine Rh) typically contain 348 amino acids arranged in seven α-helical structures. The biochemical function of Rh relies on the molecular properties of the retinal chromophore and its interactions with the surrounding amino acid environment, especially with those amino acid groups that form the retinal binding pocket. The characterization of the room-temperature Rh (Rh^{RT}) functionality in terms of the intermediates that comprise its photoreaction provides a molecular-level understanding of visual processes in both vertebrates and invertebrates. This information may also be relevant to an understanding of the corresponding intermediates that function in the much larger, heptahelical protein family (Oesterhelt, 1995).

Rh^{RT} contains an 11-*cis* retinal chromophore that is bonded to the apoprotein (opsin) via a protonated Schiff base linkage at Lys^{296} (Ovchinnikov, 1982). Light absorption by the 11-*cis* retinal in Rh^{RT} initiates isomerization to all-*trans* retinal (Wald, 1968). Recent models suggest that 11-*cis* to all-*trans* isomerization occurs on the 200-fs time scale (Wang et al., 1993, 1994; Peteanu et al., 1993; Schoenlein et al., 1991, 1993). The remainder of the Rh^{RT} photoreaction, spanning times scales from femtoseconds to milliseconds, comprises several intermediates that were initially identified via their respective absorption maxima: photo (~200 fs), batho (542 nm, ~5 ps), blue-shifted intermediate or BSI (477 nm, ~105 ns), lumi (497 nm, ~200 ns), meta I (478 nm, ~50 μs), and meta II (380 nm, ~1 ms). All of these intermediates appear and decay before the dissociation of the retinal chromophore from the apoprotein. Meta I forms an equilibrium with meta II, which is the active state for in vivo Rh^{RT} (Randall et al., 1991; Thorgeirsson et al., 1993; Lewis et al., 1992; Kliger et al., 1995). The activated Rh^{RT} functions via G-protein binding at the surface of the transmembrane protein to eventually create a synaptic signal (Franke, 1992).

The mechanistic role of $lumi^{RT}$ in the overall Rh^{RT} energy storage/transduction mechanism has not been established, although in general it is thought to function to connect the initial 11-*cis* to all-*trans* isomerization with energy transduction to the protein environment. $Lumi^{RT}$ is formed (105-ns time constant; Kliger and Lewis, 1995) from BSI^{RT} (in equilibrium with $batho^{RT}$) and decays directly to $meta^{RT}$ I (>50 μs time constant; Kliger and Lewis, 1995). The rate of the $lumi^{RT}$ to $meta^{RT}$ I transformation exhibits a strong temperature dependence, which may reflect multiexponential decay pathways with different millisecond time constants (Kliger and Lewis, 1995).

The irreversibility of the Rh^{RT} photoreaction and the wide range of time scales over which intermediates appear (vide supra) have made it exceptionally difficult to charac-

Received for publication 8 September and in final form 1 December 1997.
Address reprint requests to Dr. George H. Atkinson, Department of Chemistry, University of Arizona, P.O. Box 20041, Tucson, AZ 85721-0041. Tel.: 520-621-6293: Fax: 520-621-4858: E-mail: atkinson@ccit.arizona.edu.

0006-3495/98/03/1492/10 $2.00

terize the molecular properties of Rh^{RT} intermediates. Thus $lumi^{RT}$ had previously been identified only via transient absorption spectra. The vibrational spectrum of lumi at low temperature has been reported from Fourier transform infrared (FTIR) studies (Ganter et al., 1988, 1990, 1991), but before the PTR/CARS data presented here, no vibrational data on $lumi^{RT}$ had been reported.

The experimental challenges associated with measuring the vibrational spectrum of $lumi^{RT}$ are successfully addressed in this study with picosecond coherent anti-Stokes Raman spectroscopy (PTR/CARS). The PTR/CARS techniques and methodology were initially developed to record high-quality (S/N) vibrational data from intermediates in the room-temperature bacteriorhodopsin (BR^{RT}) photocycle (Weidlich et al., 1997; Jäger et al., 1996; Ujj et al., 1996). The subsequent application of PTR/CARS to the Rh^{RT} photoreaction independently proved to be exceptionally valuable, because it provided the first opportunities to measure high S/N vibrational spectra from intermediates in this irreversible protein reaction (e.g., $batho^{RT}$; Jäger et al., 1997; Popp et al., 1996).

This paper presents the vibrational spectrum (650 cm^{-1}-1750 cm^{-1}) of $lumi^{RT}$ and utilizes it to elucidate the retinal structure in $lumi^{RT}$ and the structural changes in the earlier stages of the Rh^{RT} photoreaction that lead to $lumi^{RT}$ formation. Comparisons of these PTR/CARS results for $lumi^{RT}$ with low-temperature FTIR spectra reported previously clarify some vibrational mode assignments for retinal and provide new insight into the related retinal-protein interactions. As a result, vibrational mode assignments, together with a geometric configuration for retinal in $lumi^{RT}$, can be derived from these data. The nano/microsecond dynamics of $lumi^{RT}$ formation are also determined independently from PTR/CARS data. Finally, PTR/CARS spectra recorded during the nanosecond appearance of $lumi^{RT}$ contain vibrational features that confirm the presence of an intermediate with a retinal structure distinct from that in either $batho^{RT}$ and $lumi^{RT}$ (e.g., BSI^{RT}).

MATERIALS AND METHODS

Bovine retinas (Lawson Co., Lincoln, NE) are prepared according to published procedures (Papermaster, 1982). The washed rod outer segments of Rh membranes are suspended in 10 mM Tris buffer (pH 7) containing aprotinin (0.1% v/v) and dithiothreitol. These samples have a ratio of 280-nm and 500-nm absorption maxima of ~2 and an optical density (OD) at 500 nm (with background scattering subtracted) of ~3. Large particle scattering from the disc membranes contributes ~2 OD (at 800 nm) to the sample absorbance. To ensure a constant Rh concentration while recording a CARS spectrum (20–30 s), the sample volume was selected to be 25–30 ml. Because the Rh concentration remains constant (<5% decrease) over the several minutes required for each PTR/CARS experiment, the amplitudes and lineshapes of CARS features remain unchanged, and therefore two consecutive CARS measurements can be averaged to improve the resultant S/N.

The instrumentation and experimental procedures used to record PTR/CARS signals are discussed in detail elsewhere (Ujj et al., 1994, 1996), and therefore only a brief description of the fundamental issues is presented here. Several instrumental enhancements specifically important to the measurements of $lumi^{RT}$ spectrum are described in detail. A schematic representation of the PTR/CARS instrumentation used is presented in Fig. 1.

The 1053-nm output (30-ps pulses at 76-MHz repetition rate) of a cw, mode-locked Nd:YLF laser (Coherent, Antares 76) is used to generate second and third harmonic radiation from LBO (527 nm) and BBO (351 nm, Coherent 7950 THG) crystals, respectively. The 527-nm and 351-nm radiation is used to pump three independently controlled dye lasers (Coherent, model 700). Each dye laser is equipped with a cavity dumper (Coherent, models 7210 and 7220), three of which are synchronized to the 76-MHz (TEM mode) repetition rate of the Nd:YLF mode locker. The entire laser system is operated at a 400-kHz repetition rate to match the flow properties of the liquid Rh^{RT} sample jet. The velocity of the Rh^{RT} sample in the 400-μm-square nozzle is adjusted to 12 m/s (laminar flow) to ensure a complete replacement of the sample volume between the arrival of sets of laser pulses. Critical to this adjustment is the beam waist of the pump beam (20 μm) and the 400-kHz repetition rate of the dye lasers.

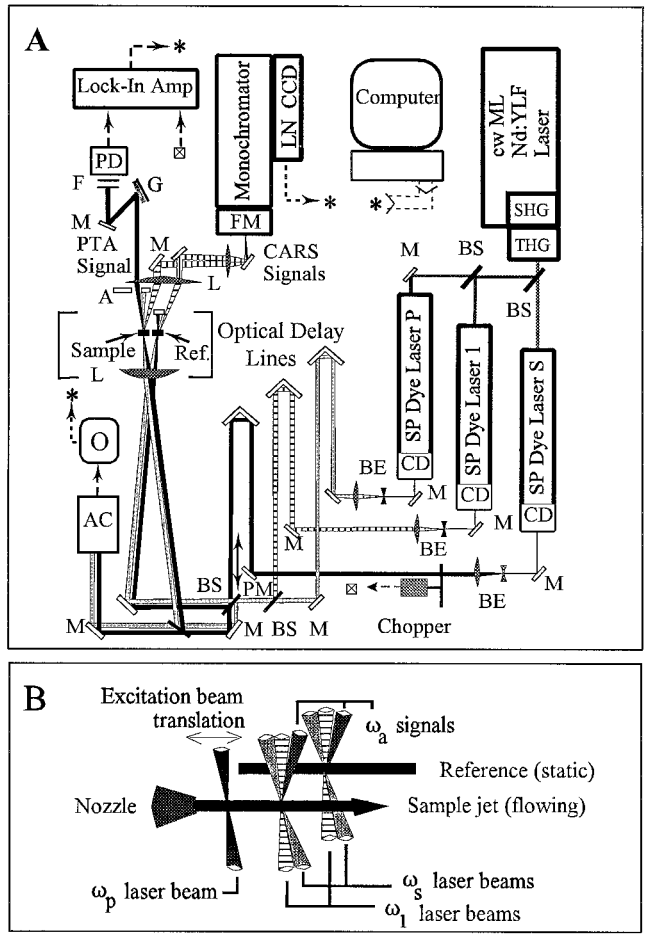

FIGURE 1 (*A*) Instrumentation used to measure PTR/CARS spectra and PTA data. SHG, second harmonic generator; THG, third harmonic generator; M, mirror; BS, beam splitter; CD, cavity dumper; BE, beam expander; AC, auto-correlator; O, oscilloscope; PD, photo diode; A, aperture; PM, phase-matching adjustment; F, optical filter; G, optical grating; L, lens. The temporal widths of the excitation and the two probe lasers pulses were 3 ps, 5.5 ps, and 7 ps, respectively (400 kHz repetition rates). (*B*) Schematic representation, based on a perspective view of the sample region indicated by the square bracket in Fig. 1 *A*, of the laser beam arrangement used to generate PTR/CARS signals. The horizontal arrow indicates adjustable spatial positions of the pump laser beam. The spatial displacement is synchronized with the timing sequence of the respective laser pulse (e.g., ω_p, ω_1, and ω_s).

A new spatial configuration of the three laser pulses used to generate PTR/CARS signals, together with a two-dimensional multichannel array detector used to measure CARS signals, is introduced into these experiments. PTR/CARS signals are generated simultaneously from two separate sample compartments, reference and Rh (Fig. 1 *B*). This new sample configuration is intended to minimize long-term intensity drift and spectral shape changes associated with the laser pulses. The reference compartment is a capillary containing a static water sample placed next to the nozzle through which the Rh^{RT} sample flows. This configuration permits the simultaneous measurement of the nonresonant background from water (Ujj et al., 1994b) and the CARS signal from Rh^{RT}, thereby minimizing the effects of any variability in the spectral intensity of the laser pulses or in the flow dynamics of the Rh^{RT} sample. The two sets of probe laser pulses required for these measurements are produced by amplitude division with a pellicle beam splitter (Fig. 1 *A*). Each pair of probe laser pulses is focused separately into the reference and sample compartments by using the same microscope objective ($f = 5$ cm). The angle between the laser beams is selected to ensure that the horizontal separation of the focal regions is ~0.8 mm. The signals from both compartments are collimated and focused onto the entrance slit of a triple monochromator (Spex, Triplemate). The wavelength-dispersed CARS signals are focused onto two separate, parallel stripes of a liquid-nitrogen-cooled, CCD multichannel array (Princeton Instruments, LN/CCD-1024-F/1 UV). The spectral resolution of these CARS measurements, determined primarily by the bandwidth of the ω_1 laser (vide infra), is <2 cm^{-1}.

The Rh^{RT} photoreaction is initiated via optical excitation (500 nm, <3-ps laser pulse, 7.5 nJ/pulse). Other than changing the relative concentrations of intermediates, no alteration in the Rh^{RT} photoreaction is found when the pumping pulse energy varies from 1 nJ to 7.5 nJ. This constancy is determined by monitoring the $batho^{RT}$ CARS signal 100 ps after excitation of Rh^{RT} as a function of the pump pulse energy (data not shown). The excitation conditions are selected to minimize any secondary photochemistry involving Rh^{RT} intermediates by utilizing 1) pump laser pulses that are short (<3 ps) relative to the appearance of $batho^{RT}$ (~5 ps), 2) probe laser wavelengths (600 nm and 626 nm-670 nm) that are on the low-energy (red) side of the absorption bands for Rh^{RT} (500 nm) and $lumi^{RT}$ (497 nm), and 3) low energies of the probe laser pulses (2 nJ and 4 nJ for ω_1 and ω_s, respectively) (Ujj et al., 1996).

Because the spectral region (542–577 nm) in which the CARS signal ($\omega_a = \omega_1 + (\omega_1 - \omega_s)$) appears is ~50 nm to the red of the one-photon absorption maximum of Rh^{RT} (500 nm with a 50-nm bandwidth, half-width half-maximum), the major resonance enhancement can be attributed to the one-photon transition at ω_a. No signals are observed that can be attributed to resonances induced by dephasing (i.e., excited-state vibrational resonances) (Andrews et al., 1981). This result is expected because ω_s is >150 nm removed from the one-photon transition in Rh^{RT}.

The temporal synchronization of the laser pulses, monitored throughout the CARS experiment with a autocorrelator (FR-103XL; Femtochrome Research), is characterized by a cross-correlation time (CCT) for the two probe laser pulses of ~9 ps. The temporal pulsewidths for ω_1 and ω_s are 5.5 ps and 7 ps, respectively (assuming Gaussian pulse envelopes). The timing jitter between the excitation pulse (ω_1) and the two probe pulses (ω_1 and ω_s) is measured to be <2 ps.

The timing sequences and delays between the three dye laser pulses are selected by three separate but correlated optical delay lines for the picosecond time scale and by electronic delays involving the three independently synchronized cavity dumpers for the nanosecond time scale (Weidlich et al., 1997). Because $lumi^{RT}$ appears in <500 ns and decays within 50 μs, a 2.5-μs delay is chosen for recording the PTR/CARS data from $lumi^{RT}$ presented here. Because the velocity of the flowing Rh^{RT} sample is adjusted to ensure that the irradiated volume is completely replaced in <2.5 μs, it is necessary to spatially displace the positions of the pump and probe laser beams within the flowing Rh^{RT} sample. Specifically, the two probe beams are displaced downstream from where the pump beam intersects the Rh^{RT} sample (Fig. 1 *B*). Coincidentally, the time interval between laser pulses is also 2.5 μs (400 kHz). Consequentially, the pump and probe laser pulses can be synchronized simply by using a pulse from the pump laser to excite the Rh^{RT} and two successive pulses from the two synchronized probe pulse trains to generate the CARS signal.

The spatial displacement of these pump and probe laser pulses is determined by monitoring the picosecond transient absorption (PTA) (Blanchard et al., 1991) signal from a BR^{RT} sample placed in the reservoir of the circulating liquid system. At 2.5-μs delay, the L-550 intermediate of the BR^{RT} photocycle is present (e.g., Lohrmann and Stockburger, 1992). The PTA signal recorded at 600 nm and at a 2.5-μs delay has an opposite sign relative to the signal assignable to the K-590 intermediate present earlier (50–100 ns) in the BR^{RT} photocycle (Ujj et al., 1996). An isobestic point for the absorption bands involved appears on the higher energy side (blue) of 600 nm. The pump/probe laser beam alignment is achieved by maximizing the PTA signal at 2.5-μs delay to ensure that the Rh^{RT} sample initially pumped is probed via CARS.

Procedurally, CARS spectra from Rh^{RT} are recorded (i.e., picosecond resonance CARS or PR/CARS) when the Rh^{RT} concentration remains unchanged. PTR/CARS data are subsequently recorded for specific time delays between the pumping pulse (ω_p) and the two probing CARS pulses (ω_1 and ω_s). PR/CARS spectra from Rh^{RT} are taken in an alternating order with PTR/CARS data to compensate for the decrease in Rh^{RT} concentration due to the irreversibility of the Rh^{RT} photoreaction.

THEORETICAL

CARS signals have complex, dispersive lineshapes that originate from interferences among the several scattered coherent waves attributable to each component of the sample (e.g., nonresonant background of the water solvent, vibrational modes within each molecular species, and resonances emanating from electronic transitions energetically accessed by the excitation wavelengths). The successful modeling of the third-order susceptibility (i.e., $\chi^{(3)}$ or the symmetrical response function in the frequency domain) of retinal protein samples utilizes two major assumptions: 1) complex Lorentzian lineshapes are accurate representations of the measured vibrational bands and 2) the electronic phase factor is constant over the relatively narrow (>300 cm^{-1}) spectral region in which CARS data are measured during a single experiment.

In general, the second assumption is not valid for electronically resonant CARS (e.g., resonance excited-state CARS; Kamalov et al., 1989), but is correct when there is correlation among the phases assigned to different vibrational modes. Because all vibrational phases are normally zero for nonresonant scattering (excitation wavelengths are energetically well removed from electronic resonances), the second assumption is correct when excitation wavelengths are on the low-energy ("red") side of the one-photon electronic absorption transitions. To a high degree of accuracy, these relationships have been confirmed empirically by using data from the ethylenic bands of BR^{RT} (Ujj et al., 1997). Based solely on the derivative lineshape in CARS data, some information, however, is lost upon $\chi^{(3)}$ analysis.

The S/N in the CARS data presented here is sufficiently large (100/1) and the spectral region measured in one experiment wide enough (~700 cm^{-1}) such that the $\chi^{(3)}$ analysis reveals some quantitative deviations from assumption 2 when the spectra are fit with a common phase value. These deviations over the entire spectral region can be readily included in the $\chi^{(3)}$ analysis by introducing a mono-

tonic phase shift via the anti-Stokes frequencies. Based on $\chi^{(3)}$ theory (Mukamel, 1995), such an ω_a dependence is expected for a simplified, condensed-phase molecular system. To accurately treat this dependence, a second-order, polynomial function of ω_a can be introduced in the $\chi^{(3)}$ susceptibility expression. An analytic formalism previously utilized [Equation 3 in (Ujj et al., 1994a)] is modified here:

$$\frac{I_a^{Rh}}{I_a^{water}} = \mu^2 \left| 1 + (1-\eta)e^{i\theta_{Rh}} \sum_{j=1}^{N_{Rh}} \frac{A_j}{\Delta_j - i} + \eta e^{i\theta_{lumi}} \sum_{k=1}^{N_{lumi}} \frac{A_k}{\Delta_k - i} \right|^2, \quad (1)$$

where a reactive mixture of Rh^{RT} (index Rh) and $lumi^{RT}$ (index lumi) is treated; $\Theta_{Rh} = \Theta_{Rh,0}(1 + a_{Rh}(\omega_a - \omega_0) + b_{Rh}(\omega_a - \omega_0)^2)$ and $\Theta_{lumi} = \Theta_{lumi,0}(1 + a_{lumi}(\omega_a - \omega_0) + b_{lumi}(\omega_a - \omega_0)^2)$ are the differences between the vibrational and background phases; a and b are the polynomial coefficients; the index 0 refers to the reference frequency (ω_0); phases ($\Theta_{Rh,0}$, $\Theta_{lumi,0}$) are chosen for the spectral region measured; μ is a scaling factor; and the summations run over the vibrational bands of Rh^{RT} (N_{Rh}) and $lumi^{RT}$ (N_{lumi}), respectively. A_j (A_k) is the amplitude and Δ_j (Δ_k) is the detuning parameter for the jth (kth) vibrational mode with a frequency Ω_j (Ω_k) and a bandwidth $2\Gamma_j$ ($2\Gamma_k$), where ($\Delta_j = (\Omega_j - (\omega_1 - \omega_s))/\Gamma_j$.). The relative concentration of $lumi^{RT}$ is given by η ($0 \leq \eta \leq 1$, but $\eta = 0$ when Rh^{RT} is not optically excited).

The degree of optical conversion from Rh^{RT} into $lumi^{RT}$ (η), estimated to be 30–35% of the original Rh^{RT} sample, is determined by the amplitude decrease in CARS bands assigned to Rh^{RT} (i.e., the decrease in the corresponding $\chi^{(3)}$ fit parameter ($1 - \eta$) for the Rh^{RT} concentration in the reactive mixture). For these quantitative $\chi^{(3)}$ analyses, the CARS spectra from Rh^{RT} and the buffer alone are normalized to the nonresonant background signal measured from the water alone (Eq. 1).

RESULTS

PR/CARS spectra of Rh^{RT} and PTR/CARS data of $lumi^{RT}$ measured in two spectrally overlapping (~700 cm^{-1} wide) regions are shown together with their respective $\chi^{(3)}$ fits in Figs. 2–5. The corresponding background-free CARS spectra (with Lorentzian lineshapes) are also presented in these figures.

Most of the features assignable to $lumi^{RT}$ are spectrally resolved in the CARS spectra measured from the reactive mixture containing Rh^{RT} and $lumi^{RT}$ (*vertical arrows* indicate bands in Figs. 3 and 5). The PR/CARS spectrum of Rh^{RT} (Figs. 2 and 4) agrees well with the corresponding resonance Raman spectrum (Mathies et al., 1977; Callender et al., 1976; Callender and Honig, 1977) and with the PR/CARS spectrum reported previously (Jäger et al., 1997). The vibrational parameters attributed to Rh^{RT} and $lumi^{RT}$ (i.e., band origin positions (Ω_i), bandwidths (Γ_i), and amplitudes (A_i)) are presented in Table 1. These band parameters are comparable to those observed in the low-temperature FTIR spectrum of lumi (Ganter et al., 1988) and in the PTR/CARS spectrum of $batho^{RT}$ (Jäger et al., 1997). A comparison with the $batho^{RT}$ spectrum is of interest, because it contains an all-*trans*, strongly twisted retinal configuration. Specific results for $lumi^{RT}$ are described for selected spectral regions.

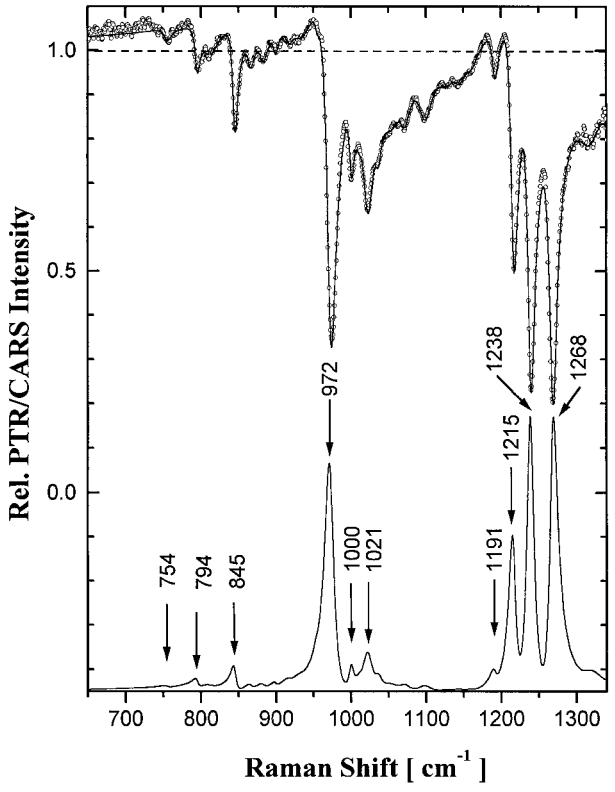

FIGURE 2 PR/CARS spectrum of Rh^{RT} (three OD sample) in the 640 cm^{-1} to 1340 cm^{-1} region. The nonresonant CARS background signal from water only, indicated by the horizontal dashed line, is used to normalize the PR/CARS signal. The phase parameters are θ^{Rh} (1100 cm^{-1}) = 67°, $a = 10^{-4}$, and $b = 10^{-8}$. The $\chi^{(3)}$-fit function (Eq. 1 with $\eta = 0$) is shown as a solid line overlapping the PR/CARS data (○). The corresponding background-free (Lorentzian lineshapes) vibrational spectrum of Rh^{RT}, as derived from the $\chi^{(3)}$ fit, is shown at the bottom. The wavenumber positions of selected bands are also presented. The ordinate for the lower spectrum is scaled arbitrarily.

Hydrogen out-of-plane and CH_3 rock vibrational region

The 650 cm^{-1} to 1000 cm^{-1} spectral region of $lumi^{RT}$ contains at least seven vibrational bands (Fig. 2) assignable to the hydrogen out-of-plane (HOOP) modes of retinal, with the most intense band located at 944 cm^{-1}. Two bands (940 cm^{-1} and 946 cm^{-1}) appear near the 944 cm^{-1} position in the low temperature (173K) FTIR spectrum (Ganter et al., 1988). Only one of these bands (947(6) cm^{-1}) is found in a recent low-temperature FTIR study in which special emphasis is placed on excluding the contribution from isorhodopsin (Maeda et al., 1993; Ohkita et al., 1995). The $batho^{RT}$

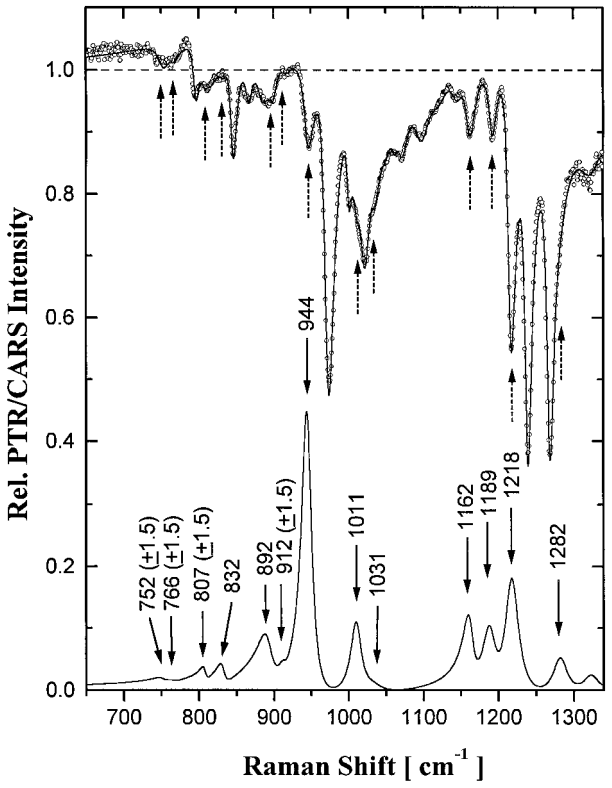

FIGURE 3 PTR/CARS spectrum in the 640 cm^{-1} to 1340 cm^{-1} region of the reaction mixture containing Rh^{RT} and $lumi^{RT}$ (37 ± 3% relative concentration) taken at 2.5 μs after photoexcitation of Rh^{RT}. The phase factors for $lumi^{RT}$ are found to be $\theta^{lum\ i}$ (1100 cm^{-1}) = 67°, $a = 10^{-4}$, and $b = 10^{-8}$. The nonresonant background signal from water and opsin, indicated by the horizontal dashed line, is used to normalize the PTR/CARS signal. The $\chi^{(3)}$ fit function (Eq. 1) is shown as a solid line overlapping the PTR/CARS data (○). The corresponding vibrational spectrum of $lumi^{RT}$, derived from the $\chi^{(3)}$ fit by using Lorentzian lineshape functions, is shown at the bottom. The origin positions of the $lumi^{RT}$ bands are indicated by arrows on each spectrum. The ordinate for the lower spectrum is scaled arbitrarily.

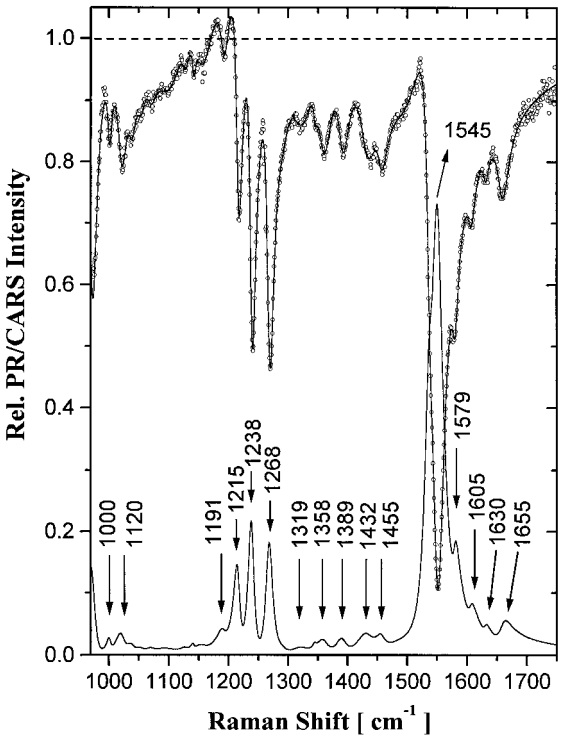

FIGURE 4 PR/CARS spectrum of Rh^{RT} (3OD sample) in the 970 cm^{-1} to 1760 cm^{-1} region. The nonresonant CARS background signal from water only, indicated by the horizontal dashed line, is used to normalize the PR/CARS signal. The phase parameters are θ^{Rh} (1300 cm^{-1}) = 70°, $a = 10^{-4}$, and $b = 10^{-8}$. The $\chi^{(3)}$ fit function (Eq. 1 with $\eta = 0$) is shown as a solid line overlapping the PR/CARS data (○). The corresponding background-free vibrational spectrum of Rh^{RT} derived from the $\chi^{(3)}$ fit is shown at the bottom. The wavenumber positions of selected bands are also presented. The ordinate for the lower spectrum is scaled arbitrarily. The asymmetrical band at 1545 cm^{-1} is fitted with two bands (see text for details).

band located at 921 cm^{-1} (Jäger et al., 1997; Eyring and Mathies, 1979) and the meta I band at 950 cm^{-1} (Doukas et al., 1978) appear to correlate with the 944 cm^{-1} lumi band. Although a definitive band near 912 cm^{-1} is not identified in FTIR spectra, a low-intensity feature appears to be present. The position and width (12 cm^{-1}) of the CARS band at 892 cm^{-1} are in agreement with this low-temperature FTIR result.

The low-intensity bands below 832 cm^{-1} found in the CARS data (Fig. 3) have not been observed previously, although the $batho^{RT}$ CARS spectrum also contains bands in this region. It is important to note that the 752 cm^{-1}/766 cm^{-1} doublet appears in the CARS spectra of Rh^{RT}, $batho^{RT}$, and $lumi^{RT}$ at essentially the same position (±2 cm^{-1}).

Two bands are also observed at 1011 cm^{-1} and 1031 cm^{-1}, with the latter appearing as a shoulder (Fig. 3). Based on the vibrational spectra assignable to the all-*trans*, protonated Schiff-base retinal in solution (Curry et al., 1982), in BR-570 (Ujj et al., 1994b; Lohrmann and Stockburger, 1992; Smith et al., 1984, 1987; Smith et al., 1987), and in $batho^{RT}$ (Jäger et al., 1997), these two bands can be tentatively assigned to the CH_3-rocking modes.

C-C stretching (fingerprint) vibrational region

The C-C stretching region contains three prominent vibrational bands at 1162 cm^{-1}, 1189 cm^{-1}, and 1217 cm^{-1}. The corresponding FTIR bands, observed as derivative features, appear at 1160 cm^{-1}, 1205.5 cm^{-1}, and 1222.5 cm^{-1}. The assignment of these bands is made by means of isotopic (^{13}C) substitutions at the C_{14} and C_{15} positions (Ganter et al., 1988). The 1162 cm^{-1} band contains mainly C_{10}-C_{11} stretching character, the 1189 cm^{-1} band is assigned as a C_{14}-C_{15} stretching mode, and the 1217 cm^{-1} band is attributable to the C_8-C_9 stretching mode. In the $batho^{RT}$ CARS spectrum, a band appearing at 1241 cm^{-1} is assigned to the C_{12}-C_{13} stretching mode (Deng et al., 1994). The analogous band for $lumi^{RT}$ is not evident, but a feature with low intensity (at least 10 times less than that of the 1162 cm^{-1} band) may be present. The fingerprint bands at 1162 cm^{-1},

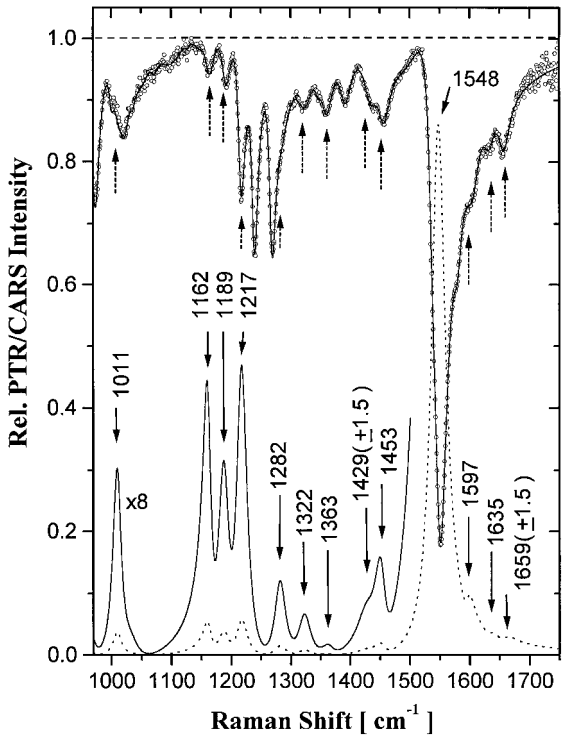

FIGURE 5 PTR/CARS spectrum in the 970 cm^{-1} to 1760 cm^{-1} region of the reaction mixture containing Rh^{RT} and $lumi^{RT}$ (37 ± 3% relative concentration) taken at 2.5 μs after photoexcitation of Rh^{RT}. The phase factors for $lumi^{RT}$ are found to be θ^{lumi} (1100 cm^{-1}) = 67°, $a = 10^{-4}$, and $b = 10^{-8}$. The nonresonant background signal from water and opsin, indicated by the horizontal dashed line, is used to normalize the PTR/CARS signal. The $\chi^{(3)}$ fit function (Eq. 1) is shown as a solid line overlapping the PTR/CARS data (○). The corresponding vibrational spectrum of $lumi^{RT}$, derived from the $\chi^{(3)}$ fit by using Lorentzian lineshape functions, is shown at the bottom. The origin positions of the $lumi^{RT}$ bands are indicated by arrows on each spectrum. The ordinate for the lower spectrum is scaled arbitrarily.

1189 cm^{-1}, and 1217 cm^{-1} are indicative of the all-*trans* retinal chromophore (Curry et al., 1982; Smith et al., 1987; Mathies et al., 1987).

The spectral region between 1250 cm^{-1} and 1400 cm^{-1} contains bands assigned to the C-C-H in-plane bending modes. At least three such bands are found at 1282 cm^{-1}, 1322 cm^{-1}, and 1363 cm^{-1}. All of these bands have a counterpart in the $batho^{RT}$ CARS spectrum (Jäger et al., 1997). In contrast, analogs to the bands near 1450 cm^{-1} observed in $lumi^{RT}$ are not found in the $batho^{RT}$ spectrum, which rather contains bands at 1427 cm^{-1} and 1453 cm^{-1}, the later being more intense.

C═C stretching (ethylenic) vibrational region

The most intense C═C stretching band in the $lumi^{RT}$ spectrum is located at 1548 cm^{-1} (Fig. 5). The excellent reproduction of the 1548-cm^{-1} bandshape by a single Lorentzian function suggests that the band is assignable to a single isolated mode. Three smaller vibrational bands are identified at 1597 cm^{-1}, 1635 cm^{-1}, and 1659-cm^{-1}.

TABLE 1 Vibrational parameters of Rh^{RT} and $lumi^{RT}$

Rhodopsin PR/CARS parameters			Lumi-rhodopsin PTR/CARS parameters		
Ω_k [cm^{-1}]	Γ_k [cm^{-1}]	A_k	Ω_k [cm^{-1}]	Γ_k [cm^{-1}]	A_k
752	9	0.015	752	9	0.015
770	7	0.010	766	7	0.007
780	7	0.029			
814	15	0.034	807	5	0.036
846	5	0.097	832	6	0.053
867	11	0.053			
883 ± 2	6	0.030	892	12	0.101
900 ± 3	10	0.030			
923	10	0.019	912	5	0.018
938	8	0.025	944	8	0.369
972	9	0.42			
1000	5	0.083			
1010	7	0.054	1010	9	0.170
1021	8	0.16			
1035 ± 2	8	0.065	1031	16	0.031
1050 ± 3	11	0.046			
1071	9	0.055			
1097	15	0.050			
1145 ± 3	15	0.055	1162	8	0.161
1190	9	0.088	1189	10	0.138
1214	7	0.33	1217	11	0.210
1232	4	0.15			
1238	5	0.41			
1267	7	0.46	1282	12	0.101
1316	12	0.058	1322	13	0.071
1345	8	0.039			
1359	10	0.10	1362	13	0.025
1390	11	0.096			
1434	15	0.11	1429	16	0.030
1459	15	0.074	1452	11	0.078
1486	18	0.037			
1507	15	0.033			
1536	11	0.44			
1548	10	0.68	1547	14	0.910
1578	7	0.10			
1604	7	0.069	1597	7	0.070
1631	8	0.030	1635	7	0.023
1655	8	0.065	1659	10	0.032

Parameters (Ω_k, band origin; Γ_k, bandwidth HWHM; A_k, amplitudes) from the $\chi^{(3)}$ fit of the CARS spectra (640 cm^{-1} to 1750 cm^{-1}) for Rh^{RT} and $lumi^{RT}$ presented in Figs. 1–4. The values for the PR/CARS amplitudes represent typical values for a 3–4 OD sample if the spectrum is normalized to the nonresonant CARS background. The values for the PTR/CARS amplitudes correspond to a 3–4 OD sample with 35–40% conversion to intermediates via optical excitation.

The $\chi^{(3)}$ analysis of these bands reveals that the 1545 cm^{-1} feature in Rh^{RT} (Fig. 4) is composed of two bands (at 1536 cm^{-1} and 1547 cm^{-1} (Jäger et al., 1997)). Regardless of whether one or two bands are assumed to be present in the 1545 cm^{-1} feature of Rh^{RT}, the $lumi^{RT}$ band extracted from the PTR/CARS data remains unchanged (±0.5 cm^{-1}) at 1548 cm^{-1}, and only the amplitude of the band is altered, by ~15%. The appearance of a 1548 cm^{-1} band in the $lumi^{RT}$ spectrum is consistent with the correlation between the absorption shift (i.e., "opsin shift") and the C═C stretching frequency (Jäger et al., 1997; Kakitani et al., 1983). For Rh^{RT} and $lumi^{RT}$, the respective absorption

maxima are not significantly different (<5 nm), and therefore the small (<2 cm^{-1}) shift observed is expected. The C═N stretching (Schiff base) mode appears to be shifted ~3–7 cm^{-1} (1659 ± 1.5 cm^{-1}) relative to the band position found in batho^{RT} (1653 ± 1.5 cm^{-1}) (Jäger et al., 1997).

Low-temperature FTIR spectra of lumi contain several bands in the 1500–1800 cm^{-1} region (Ganter et al., 1988). Based on the CARS data presented here, it is evident that, other than the bands described here, all of the 1500–1800 cm^{-1} bands are assignable to vibrational modes in the peptide chain (e.g., amide-I and -II and carboxylic acids).

DISCUSSION

Retinal configuration in lumi^{RT}

The mechanistic contribution made by lumi^{RT} to the overall Rh^{RT} photoreaction involves the transfer of the initial 33 kcal/mol (Schick et al., 1987; Birge et al., 1989; Cooper, 1979) stored in batho^{RT} to the protein. The specific retinal/protein interactions utilized are not yet fully characterized, but may involve even the tertiary structure of the protein, including changes in the cytoplasmic LOOP region of Rh^{RT}. The formation of intermediates late in the Rh^{RT} photoreaction such as lumi^{RT} are thought to be key elements in this transfer of energy from the retinal structure to the protein.

The retinal configuration in lumi^{RT} can be characterized primarily via the CARS spectrum presented here:

1. HOOP bands suggest that the retinal has a planar geometry and is not significantly twisted out of plane.

2. Fingerprint bands suggest that retinal configuration is all-*trans*.

3. The C═C band frequencies indicate that the charge delocalization within the lumi^{RT} binding pocket is similar to that in Rh^{RT}, but different from that in batho^{RT}.

These general conclusions are based on the following specific observations and comparisons.

Vibrational band assignments in lumi^{RT}

1. The vibrational band pattern in the HOOP region of the lumi^{RT} spectrum is similar to that measured from all-*trans*, protonated Schiff base retinal in solution (Curry et al., 1982). The exception is that no band near 960 cm^{-1} appears in the lumi^{RT} spectrum.

2. Tentatively, the 944 cm^{-1} band in lumi^{RT} can be assigned primarily to the "A_u" HC_{11}-$C_{12}H$ mode, although contributions from other HOOP modes can not be completely excluded. Coupling of the HC_{11}-$C_{12}H$ mode with the C_{13}-methyl group may also be involved (Koch and Gartner, 1997; Ganter et al., 1990). This assignment of the 944 cm^{-1} band is consistent with the low-temperature assignment (Ohkita et al., 1995).

3. In low-temperature FTIR spectra (Ganter et al., 1988), bands other than those observed in CARS data appear in the 856–920 cm^{-1} region. Their absence from the CARS spectrum of lumi^{RT} suggests that these vibrations reflect a smaller, tighter protein binding pocket at low temperature than that present at room temperature. Such changes in the coupling between the retinal chromophore and the apoprotein may be accentuated by the localized twisting of the carbon chain, which could alter steric interactions between retinal and a specific amino acid group (e.g., a methyl group and an amino acid comprising the binding pocket).

Comparison between lumi^{RT} and batho^{RT}

1. The strong HOOP band (850–870 cm^{-1}) intensities in the CARS spectrum of batho^{RT} (Jäger et al., 1997) clearly indicate that the polyene chain is twisted (i.e., enhanced polarizability changes). This polyene backbone twisting disappears when batho^{RT} converts (presumably through BSI^{RT}) into lumi^{RT}. The relationship between the HOOP band intensities and the degree of twisting at specific, localized C═C-C bonds has been well established from both Raman and IR studies (Deng et al., 1991; Curry et al., 1982; Eyring et al., 1982).

2. The C_{12}-H and C_{11}-H wagging vibrations, decoupled from each other in batho^{RT}, are assigned in batho^{RT} to the bands at 856 cm^{-1} and 920 cm^{-1}, respectively. Because only one intense band at 944 cm^{-1} is observed in the lumi^{RT} spectrum, these wagging modes appear to become recoupled during the batho^{RT} to lumi^{RT} transformation. The analogous band in the low-temperature FTIR spectrum appears at 947 cm^{-1} and is assigned by means of isotopic substitutions (deuterations at the C_{12} and C_{14} positions) to modes containing contributions from both C_{11}-HOOP and C_{12}-HOOP vibrations. Based on this assignment of the 947 cm^{-1} band, the room- and low-temperature retinal HOOP modes are found to be the same.

3. The fingerprint bands show that the overall retinal configuration (i.e., all-*trans*) in batho^{RT} is not altered in lumi^{RT}. This is consistent with the view that lumi^{RT} is associated with changes in the retinal/protein interactions and that the primary structural changes in retinal during the early stages of the Rh^{RT} photoreaction occur as batho^{RT} is formed from Rh^{RT}.

4. The C═C stretching bands are significantly different in batho^{RT} and lumi^{RT}. For example, the most intense band at 1533 cm^{-1} for batho^{RT} (Jäger et al., 1997) shifts to 1548 cm^{-1} in lumi^{RT}. Because the frequency of the C═C stretching mode reflects the degree of electronic charge delocalization along the entire retinal polyene chain, it is reasonable to conclude that the molecular parameters that influence electron delocalization (e.g., charge separation) are fundamentally altered as lumi^{RT} is formed from batho^{RT}.

If it is assumed that the primary parameters affecting electron delocalization involve interaction between the Schiff-base nitrogen and the counterion (Glu^{113}) in the protein binding pocket (Jäger et al., 1994; Han et al., 1993; Han and Smith, 1994, 1995a,b), then the increase in the C═C stretching frequency indicates that the C═N-H/Glu^{113} distance decreases substantially when lumi^{RT} is

formed. This conclusion is consistent with the blue shift in the absorption maximum of lumi^{RT} relative to that of batho^{RT}.

Comparison of lumi^{RT} and Rh^{RT}

1. When the vibrational CARS spectra of Rh^{RT} and lumi^{RT} are compared directly (Fig. 7), it is evident that the two species contain distinct retinal structures: Rh^{RT} with 11-*cis* and lumi^{RT} with all-*trans*. The vibrational spectra of all-*trans*, 13-*cis*, and 11-*cis* retinal in solution have been analyzed extensively to determine characteristic vibrational patterns assignable to specific retinal isomers (Curry et al., 1982, 1984; Eyring et al., 1982). Comparisons of the HOOP and fingerprint bands support this conclusion.

2. There is only a small increase (<3 cm^{-1}) in the C═C frequency in lumi^{RT} (1548 cm^{-1}) versus Rh^{RT} (1545 cm^{-1}). Considering the charge delocalization arguments (vide supra), it is reasonable to conclude that the net effect of the molecular parameters that influence electron delocalization (e.g., charge separation) are essentially the same in lumi^{RT} and Rh^{RT}. For example, the small change in the C═C stretching frequency indicates that, at most, the C ═ N-H/Glu^{113} distance decreases slightly when lumi^{RT} is formed. This conclusion is consistent with the <5-nm blue shift in the absorption maximum observed for the Rh^{RT} to lumi^{RT} transformation (Kliger and Lewis, 1995). Although not obvious, other changes in these molecular parameters may also underlie the similarity of C═C stretching frequencies observed in lumi^{RT} and Rh^{RT}.

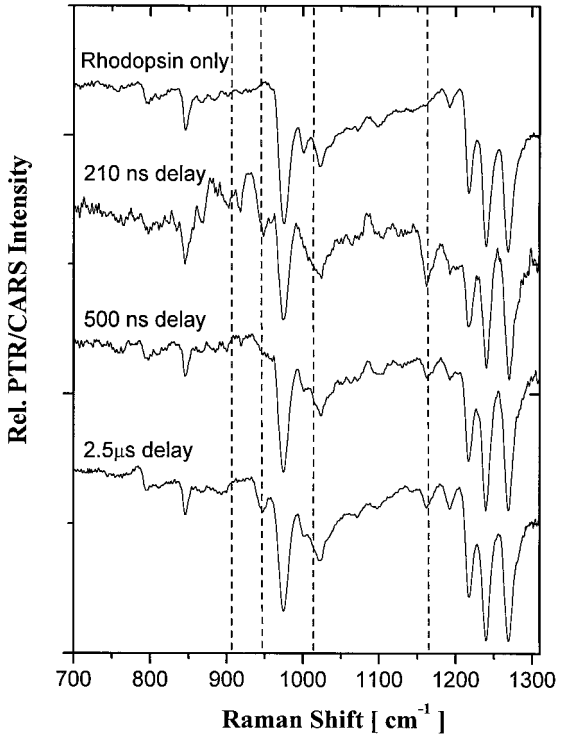

FIGURE 6 PR/CARS spectrum (640 cm^{-1} to 1300 cm^{-1}) of Rh^{RT} in water (upper) and PTR/CARS spectra of reactive mixtures containing Rh^{RT} and its photoreaction intermediates recorded 210 ns, 500 ns, and 2.5 μs after photoexcitation (500 nm, 3 ps, 7.5 nJ) of Rh^{RT}. The vertical dashed lines indicate the most prominent, time-dependent spectral changes.

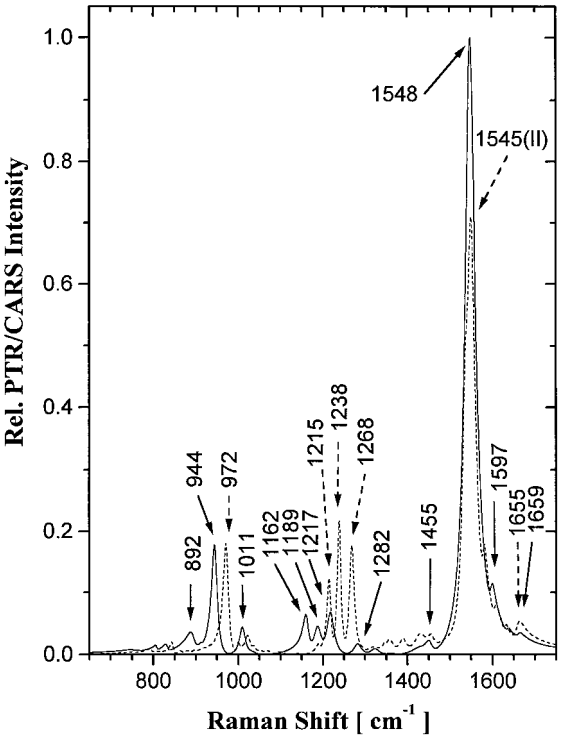

FIGURE 7 Background-free (Lorentzian lineshape) vibrational spectrum of Rh^{RT} (– – –) and lumi^{RT} (——) over the 750 cm^{-1}–1750 cm^{-1} region. The ordinate scale for the lumi^{RT} spectrum is normalized to 1. The intensity of the 972-cm^{-1} band in the spectrum of Rh^{RT} is normalized to the intensity of the 944-cm^{-1} band in the lumi^{RT} spectrum. The origin positions of the most significant bands are indicated by arrows.

Appearance of lumi^{RT} and BSI^{RT}

Transient absorption studies have shown that lumi^{RT} is formed with a 105-ns time constant. Lumi^{RT} is preceded in the Rh^{RT} photoreaction by the batho^{RT}/BSI^{RT} equilibrium (batho^{RT} $\rightarrow$ BSI^{RT} (74 ns) and BSI^{RT} $\rightarrow$ batho^{RT} (107 ns) (Kliger and Lewis, 1995)). The >50-μs time constant with which lumi^{RT} decays to meta^{RT} I exhibits a strong temperature dependence that may reflect multiexponential decay processes extending into the millisecond time regime (Kliger and Lewis, 1995).

PTR/CARS spectra measured with time delays of 210 ns, 500 ns, and 2.5 μs (Fig. 6) reveal significant spectral differences (highlighted by *dashed lines*) that indicate time-dependent changes in the reactive mixture of Rh^{RT} intermediates monitored. Specifically, the PTR/CARS spectrum recorded at 210 ns should contain vibrational band(s) assignable to batho^{RT} and BSI^{RT}, whereas the spectrum recorded at 2.5 μs should contain a vibrational structure assignable to lumi^{RT} and Rh^{RT}. Only lumi^{RT} and Rh^{RT} bands are also anticipated to contribute to the 500-ns PTR/

CARS spectrum, because the lumi^{RT} concentration should be significantly less at 500 ns than at 2.5 μs.

Because the 210-ns spectrum contains both batho^{RT} and BSI^{RT} contributions, the CARS lineshapes are especially complex. From the quantitative utilization of the PTR/CARS spectrum of batho^{RT} measured previously (Jäger et al., 1997), it is evident that BSI^{RT} bands appear near 944 cm^{-1}, 1162 cm^{-1}, and 1000 cm^{-1}. The 210-ns spectrum also contains bands in the 850–950 cm^{-1} region that are not found in Rh^{RT}, batho^{RT}, or lumi^{RT} spectra. The intensities of bands common to the 210-ns and batho^{RT} spectra are significantly reduced in the former.

Some information on the retinal structure in BSI^{RT} can be derived from even these few vibrational features. Like batho^{RT}, BSI^{RT} appears to have an all-*trans* retinal. The twisted retinal chain found in batho^{RT} is relaxed in BSI^{RT}, but is not completely planar and static relative to out-of-plane motion. The change in the CH_3-rocking region (1000–1050 cm^{-1}) suggests that retinal/protein interactions are stronger in BSI^{RT} than in batho^{RT}, an effect that may be important in establishing the batho^{RT} $\leftrightarrow$ BSI^{RT} equilibrium.

Mechanistic role of lumi^{RT}

The PTR/CARS spectra of lumi^{RT} presented here provide new insight into the role of this intermediate in the Rh^{RT} photoreaction. The formation of lumi^{RT} from BSI^{RT} appears to primarily involve a spatial accommodation for the relaxed (nontwisted) all-*trans* retinal within the protein binding pocket. It should be noted that low-temperature FTIR data suggest that the retinal in lumi^{RT} interacts strongly with the peptide chain (Ganter et al., 1991). Most of the optical energy absorbed by Rh^{RT} has previously been transferred to/stored within batho^{RT} and utilized in the batho^{RT} $\leftrightarrow$ BSI^{RT} equilibrium. The latter may involve mostly the transfer of energy from the retinal structure into the protein, although this model requires more detailed examination via methods such as PTR/CARS.

The authors thank Mr. Anthony Mazza and Mr. Hameed Shaukat for their technical assistance in the preparation of rhodopsin samples.

This research is supported by a grant to GHA from the National Institutes of Health (GM46439). FJ gratefully acknowledges the Deutscher Akademischer Austausch Dienst for the award of a DAAD/NATO postdoctoral fellowship and the University of Arizona Foundation for financial assistance.

REFERENCES

Andrews, J. R., and R. M. Hochstrasser. 1981. Thermally induced excited-state coherent Raman spectra of solids. *Chem. Phys. Lett.* 82:381–385.

Birge, R. R., T. M. Cooper, A. F. Lawrence, M. B. Masthay, C. Vasilakis, C.-F. Zhang, and R. Zidovetzki. 1989. A spectroscopic photocalorimetric and theoretical investigation of the quantum efficiency of the primary event in bacteriorhodopsin. *J. Am. Chem. Soc.* 111:4063–4074.

Blanchard, D., D. A. Gilmore, T. L. Brack, H. Lemaire, D. Hughes, and G. H. Atkinson. 1991. Picosecond time-resolved absorption and fluorescence in the bacteriorhodopsin photocycle: vibrationally-excited species. *Chem. Phys.* 156:155–170.

Callender, R. H., A. G. Doukas, R. K. Crouch, and K. Nakanishi. 1976. Molecular flow resonance Raman effect from retinal and rhodopsin. *Biochemistry.* 15:1621–1629.

Callender, R. H., and B. Honig. 1977. Resonance Raman studies of visual pigments. *Annu. Rev. Biophys. Bioeng.* 6:33–55.

Cooper, A. 1979. Energy uptake in the first step of visual excitation. *Nature.* 282:531–533.

Curry, B., A. Broek, J. Lugtenburg, and R. A. Mathies. 1982. Vibrational Analysis of all-*trans*-retinal. *J. Am. Chem. Soc.* 104:5274–5286.

Curry, B., I. Palings, A. Broek, J. A. Pardoen, P. P. J. Mulder, J. Lugtenburg, and R. Mathies. 1984. Vibrational analysis of 13-*cis*-retinal. *J. Phys. Chem.* 88:688–702.

Deng, H., L. Huang, M. Groesbeek, J. Lugtenburg, and R. H. Callender. 1994. Vibrational analysis of a retinal protonated Schiff base analog. *J. Phys. Chem.* 98:4776–4779.

Deng, H., D. Manor, G. Weng, P. Rath, Y. Koutalos, T. Ebrey, R. Gebhard, J. Lugtenburg, M. Tsuda, and R. H. Callender. 1991. Resonance Raman studies of the HOOP modes in octopus bathorhodopsin with deuterium-labeled retinal chromophores. *Biochemistry.* 30:4495–4502.

Doukas, A. G., R. H. Callender, and T. G. Ebrey. 1978. Resonance Raman studies of bovine metarhodopsin I and metarhodopsin II. *Biochemistry.* 17:2430–2435.

Eyring, G., B. Curry, A. Broek, J. Lugtenburg, and R. Mathies. 1982. Assignment and interpretation of hydrogen out-of-plane vibrations in the resonance Raman spectra of rhodopsin and bathorhodopsin. *Biochemistry.* 21:384–393.

Eyring, G., and R. A. Mathies. 1979. Resonance Raman studies of bathorhodopsin: evidence for a protonated Schiff base linkage. *Proc. Natl. Acad. Sci. USA.* 76:33–37.

Franke, R. R., T. P. Sakmar, R. M. Graham, and H. G. Khorana. 1992. Structure and function in rhodopsin. Studies of the interaction between the rhodopsin cytoplasmic domain and transducin. *J. Biol. Chem.* 267: 14767–14774.

Ganter, U. M., W. Gärtner, and F. Siebert. 1988. Rhodopsin-lumirhodopsin phototransition of bovine rhodopsin investigated by Fourier transform infrared difference spectroscopy. *Biochemistry.* 27:7480–7488.

Ganter, U. M., W. Gärtner, and F. Siebert. 1990. The influence of the 13-methyl group of the retinal on the photoreaction of rhodopsin revealed by FTIR difference spectroscopy. *Eur. Biophys. J.* 18:295–299.

Ganter, U. M., C. Longstaff, M. A. Pajares, R. R. Rando, and F. Siebert. 1991. Fourier transform infrared studies of active-site-methylated rhodopsin. *Biophys. J.* 59:640–644.

Han, M., B. S. DeDecker, and S. O. Smith. 1993. Localization of the retinal protonated Schiff base counterion in rhodopsin. *Biophys. J.* 65:899–906.

Han, M., and S. O. Smith. 1994. Location of the Schiff base counterion in the bovine rhodopsin retinal binding site. *In* Thirty-Eighth Annual Meeting of the Biophysical Society, New Orleans, LA, March 6–10, 1994. A46.

Han, M., and S. O. Smith. 1995a. High-resolution structural studies of the retinal-glu^{113} interaction in rhodopsin. *Biophys. Chem.* 56:23–29.

Han, M., and S. O. Smith. 1995b. NMR constraints on the location of the retinal chromophore in rhodopsin and barthorhodopsin. *Biochemistry.* 34:1425–1432.

Jäger, F., S. Jäger, O. Kräutle, N. Friedman, M. Sheves, K. P. Hofmann, and F. Siebert. 1994. Interactions of the beta-ionone ring with the protein in the visual pigment rhodopsin control the activation mechanism. An FTIR and fluorescence study on artifical vertebrate rhodopsins. *Biochemistry.* 33:7389–7397.

Jäger, F., L. Ujj, and G. H. Atkinson. 1997. Vibrational spectrum of batho in the room-temperature rhodopsin photo-reaction. *J. Am. Chem. Soc.* (in press).

Jäger, F., L. Ujj, G. H. Atkinson, M. Sheves, N. Livnah, and M. Ottolenghi. 1996. Vibrational spectrum of K-590 containing $^{13}C_{14,15}$ retinal: picosecond time-resolved coherent anti-Stokes Raman spectroscopy of the room temperature bacteriorhodopsin photocycle. *J. Phys. Chem.* 100: 12066–12075.

Kakitani, K., T. Kakitani, H. Rodman, B. Honig, and R. Callender. 1983. Correlation of vibrational frequencies with absorption maxima in polyenes, rhodopsin, bacteriorhodopsin, and retinal analogues. *J. Phys. Chem.* 87:3620–3628.

Kamalov, V. F., N. I. Koroteev, and B. N. Toleutaev. 1989. Picosecond coherent Raman spectroscopy of excited electronic states of multiatomic molecules in solutions. *In* Time Resolved Spectroscopy. R. J. H. Clark and R. E. Hester, editors. John Wiley and Sons, New York. 255–299.

Kliger, D. S., and J. W. Lewis. 1995. Spectral and kinetic characterization of visual pigment photointermediates. *Isr. J. Chem.* 35:289–307.

Koch, D., and W. Gartner. 1997. Steric hundrance between chromophore substituents as the driving force of rhodopsin photoisomerization: 10-methyl-13-demethyl retinal containing rhodopsin. *Photochem. Photobiol.* 65:181–186.

Lewis, J. W., and D. S. Kliger. 1992. Photointermediates of visual pigments. *J. Bioenerg. Biomembr.* 24:201–210.

Lohrmann, R., and M. Stockburger. 1992. Time-resolved resonance Raman studies of bacteriorhodopsin and its intermediates K_{590} and L_{550}: biological implications. *J. Raman Spectrosc.* 23:575–583.

Maeda, A., Y. J. Ohkita, J. Sasaki, Y. Shichida, and T. Yoshizawa. 1993. Water structural changes in lumirhodopsin, metarhodopsin I, and metarhodopsin II upon photolysis of bovine rhodopsin: analysis by Fourier transform infrared spectroscopy. *Biochemistry.* 32:12033–12038.

Mathies, R. A. 1977. Resonance Raman studies of the conformation of retinal in rhodopsin and isorhodopsin. *J. Mol. Biol.* 109:367–372.

Mathies, R. A., S. O. Smith, and I. Palings. 1987. Determination of retinal chromophore structure in rhodopsins. *In* Biological Applications of Raman Spectroscopy. T. G. Spiro, editor. John Wiley and Sons, New York. 59–108.

Mukamel, S. 1995. Principles of Nonlinear Optical Spectroscopy. New York, Oxford University Press, Inc.

Oesterhelt, D. 1995. Structure and function of halorhodopsin. *Isr. J. Chem.* 35:475–494.

Ohkita, Y. J., J. Sasaki, A. Maeda, T. Yoshizawa, M. Groesbeek, P. Verdegern, and J. Lugtenburg. 1995. Changes in structure of the chromophore in the photochemical process of bovine rhodopsin as revealed by FTIR spectroscopy for hydrogen out-of-plane vibrations. *Biophys. Chem.* 56(1–2):71–78.

Ovchinnikov, Y. A. 1982. Rhodopsin and bacteriorhodopsin: structure–function relationships. *FEBS Lett.* 148:179–191.

Papermaster, D. S. 1982. Preparation of retinal rod outer segments. *Methods Enzymol.* 81:48–52.

Peteanu, L. A., R. W. Schoenlein, Q. Wang, R. A. Mathies, and C. V. Shank. 1993. The first step in vision occurs in femtoseconds: complete blue and red spectral studies. *Proc. Natl. Acad. Sci. USA.* 90: 11762–11766.

Popp, A., L. Ujj, and G. H. Atkinson. 1996. Bathorhodopsin structure in the room-temperature rhodopsin photosequence: picosecond time-resolved coherent anti-Stokes Raman scattering. *Proc. Natl. Acad. Sci. USA.* 93:372–376.

Randall, C. E., J. W. Lewis, S. J. Hug, S. C. Björling, I. Eisner-Shanas, N. Friedman, M. Ottolenghi, M. Sheves, and D. S. Kliger. 1991. A new photolysis intermediate in artificial and native visual pigments. *J. Am. Chem. Soc.* 113:3473–3485.

Schick, G. A., T. M. Cooper, R. A. Holloway, L. P. Murray, and R. R. Birge. 1987. Energy storage in the primary photochemical events of rhodopsin and isorhodopsin. *Biochemistry.* 26:2556–2562.

Schoenlein, R. W., L. A. Peteanu, R. A. Mathies, and C. V. Shank. 1991. The first step in vision: femtosecond isomerization of rhodopsin. *Science.* 254:412–415.

Schoenlein, R. W., L. A. Peteanu, Q. Wang, R. A. Mathies, and C. V. Shank. 1993. Femtosecond dynamics of *cis-trans* isomerization in a visual pigment analog: isorhodopsin. *J. Phys. Chem.* 97:12087–12092.

Smith, S. O., M. Braiman, A. B. Myers, J. A. Pardoen, J. M. Courtin, C. Winkel, J. Lugtenburg, and R. A. Mathies. 1987. Vibrational analysis of the all-*trans* retinal chromophore in light-adapted bacteriorhodopsin. *J. Am. Chem. Soc.* 109:3108–3125.

Smith, S. O., A. B. Myers, J. A. Pardoen, C. Winkel, P. P. J. Mulder, J. Lugtenburg, and R. Mathies. 1984. Determination of retinal Schiff base configuration in bacteriorhodopsin. *Proc. Natl. Acad. Sci. USA.* 81: 2055–2059.

Thorgeirsson, T. E., J. W. Lewis, S. E. Wallace-Williams, and D. S. Kliger. 1993. Effects of temperature on rhodopsin photointermediates from lumirrhodopsin to metarhodopsin II. *Biochemistry.* 32:13861–13872.

Ujj, L., F. Jäger, A. Popp, and G. H. Atkinson. 1996. Vibrational spectrum of the K-590 intermediate in the bacteriorhodopsin photocycle at room temperature: picosecond time-resolved resonance coherent anti-Stokes Raman spectroscopy. *Chem. Phys.* 212:421–436.

Ujj, L., A. Popp, and G. H. Atkinson. 1994a. Picosecond resonance coherent anti-Stokes Raman spectroscopy of bacteriorhodopsin: quantitative third-order susceptibility analysis of the dark-adapted mixture. *Chem. Phys.* 188:221–234.

Ujj, L., A. Popp, F. Jäger, R. Ligon, and G. H. Atkinson. 1997. Picosecond time-resolved resonance coherent anti-Stokes Raman spectroscopy of bacteriorhodopsin: experimental challenges and the K-590 spectrum. Los Alamos National Laboratory UC-901, UC-910:281–282.

Ujj, L., B. L. Volodin, A. Popp, J. K. Delaney, and G. H. Atkinson. 1994b. Picosecond resonance coherent anti-Stokes Raman spectroscopy of bacteriorhodopsin: spectra and quantitative third-order susceptibility analysis of the light-adapted BR-570. *Chem. Phys.* 182:291–311.

Wald, G. 1968. Molecular basis of visual excitation. *Science.* 162: 230–239.

Wang, Q., R. W. Schoenlein, L. A. Peteanu, R. A. Mathies, and C. V. Shank. 1993. Femtosecond dynamics of the cis-trans isomerization in rhodopsin the first step in vision. *In* Thirty-Seventh Annual Meeting of the Biophysical Society, Washington, DC, February 14–18, 1993. A127.

Wang, Q., R. W. Schoenlein, L. A. Peteanu, R. A. Mathies, and C. V. Shank. 1994. Vibrationally coherent photochemistry in the femtosecond primary event of vision. *Science.* 266:422–424.

Weidlich, O., L. Ujj, F. Jäger, and G. H. Atkinson. 1997. Nanosecond retinal structure changes in K-590 during the room-temperature bacteriorhodopsin photocycle: picosecond time-resolved coherent anti-Stokes Raman spectroscopy. *Biophys. J.* 72:2329–2341.